

NEAR-INFRARED AND STAR-FORMING PROPERTIES OF LOCAL LUMINOUS INFRARED GALAXIES

ALMUDENA ALONSO-HERRERO,¹ GEORGE H. RIEKE,² MARCIA J. RIEKE,² LUIS COLINA,¹
PABLO G. PÉREZ-GONZÁLEZ,² AND STUART D. RYDER³
Received 2006 March 10; accepted 2006 June 3

ABSTRACT

We use *Hubble Space Telescope* (*HST*) NICMOS continuum and Pa α observations to study the near-infrared and star formation properties of a representative sample of 30 local ($d \sim 35\text{--}75$ Mpc) luminous infrared galaxies (LIRGs, infrared $[8\text{--}1000 \mu\text{m}]$ luminosities of $\log L_{\text{IR}} = 11\text{--}11.9 L_{\odot}$). The data provide spatial resolutions of 25–50 pc and cover the central $\sim 3.3\text{--}7.1$ kpc regions of these galaxies. About half of the LIRGs show compact ($\sim 1\text{--}2$ kpc) Pa α emission with a high surface brightness in the form of nuclear emission, rings, and minispirals. The rest of the sample show Pa α emission along the disk and the spiral arms extending over scales of 3–7 kpc and larger. About half of the sample contains H II regions with H α luminosities significantly higher than those observed in normal galaxies. There is a linear empirical relationship between the mid-IR 24 μm and hydrogen recombination (extinction-corrected Pa α) luminosity for these LIRGs, and the H II regions in the central part of M51. This relation holds over more than four decades in luminosity, suggesting that the mid-IR emission is a good tracer of the star formation rate (SFR). Analogous to the widely used relation between the SFR and total IR luminosity of R. Kennicutt, we derive an empirical calibration of the SFR in terms of the monochromatic 24 μm luminosity that can be used for luminous, dusty galaxies.

Subject headings: galaxies: interactions — galaxies: ISM — galaxies: spiral — galaxies: star clusters —
H II regions — infrared: galaxies

Online material: color figures, extended figure set

1. INTRODUCTION

The importance of infrared (IR) bright galaxies has been recognized since their discovery more than 30 years ago (Rieke & Low 1972) and their detection in large numbers by the *IRAS* satellite (Soifer et al. 1987). Specifically, there has been controversy over the extent to which luminous and ultraluminous IR galaxies (LIRGs, $L_{\text{IR}} = L[8\text{--}1000 \mu\text{m}] = 10^{11}\text{--}10^{12} L_{\odot}$, and ULIRGs $L_{\text{IR}} > 10^{12} L_{\odot}$, respectively) in the local universe are powered by intense star formation as opposed to active galactic nuclei (see the review by Sanders & Mirabel 1996). The process of merging with accompanying superstarbursts that produces LIRGs and ULIRGs appears to be an important stage in galaxy evolution, possibly even converting spiral galaxies into ellipticals (e.g., Genzel et al. 2001; Colina et al. 2001, and references therein) and giving rise to quasars (Sanders et al. 1988).

In recent years with the advent of the new generation of IR satellites, there has been considerable effort devoted to understanding the properties of distant IR-selected galaxies. The majority of these galaxies at $z < 1$ are in the LIRG class, and they make a significant contribution to the star formation rate density at $0.5 < z < 2$ (Elbaz et al. 2002; Pérez-González et al. 2005; Le Flocc'h et al. 2005). At $z \sim 0.7\text{--}1$ a significant fraction of the LIRG population appears to be morphologically disturbed spiral galaxies (Bell et al. 2005; Shi et al. 2006), rather than interacting and merging systems. These high- z IR-bright galaxies show morphologies and properties (see e.g., Zheng et al. 2004; Papovich et al. 2005; Melbourne et al. 2005; Shi et al. 2006)

typical of low- z LIRGs and ULIRGs (among others, Murphy et al. 1996; Surace et al. 2000; Scoville et al. 2000; Alonso-Herrero et al. 2002; Colina et al. 2001, 2004; Arribas et al. 2004). Lagache et al. (2005) have recently reviewed the properties of the high- z IR galaxy population.

The local density of LIRGs is 2 orders of magnitude higher than that of ULIRGs (e.g., Soifer et al. 1987). Moreover, Murphy et al. (2001) have argued that in the local universe interacting galaxies may spend a significant fraction of their lifetime as LIRGs, whereas the ULIRG phase may just be short and recurrent during the merging process. However, the majority of the detailed studies of the local universe IR galaxies have focused on the objects with the largest IR luminosities (i.e., ULIRGs). The LIRGs have been generally neglected, except for detailed studies of a few famous examples (e.g., Gehrz et al. 1983; Doyon et al. 1994; Genzel et al. 1995; Satyapal et al. 1999; Sugai et al. 1999; Lípári et al. 2000, 2004; Alonso-Herrero et al. 2000, 2001). Thus, understanding low- z LIRG samples is critical for interpreting the properties of IR-selected high- z galaxy populations; in addition, they represent the link between ULIRGs and the population of field galaxies as a whole.

In this paper we present *Hubble Space Telescope* (*HST*) NICMOS continuum (1.1, 1.6, and 1.876 μm) and Pa α emission-line observations of a volume-limited sample (30 systems, 34 individual galaxies) of local universe ($z < 0.017$) LIRGs. The paper is organized as follows. Section 2 gives details on the sample selection and properties. In § 3 we describe the *HST* NICMOS observations, data reduction, and continuum and H II region photometry. In § 4 we discuss the near-IR continuum properties of the central regions of local LIRGs. In § 5, and § 6, we describe the Pa α morphology, and the properties of individual H II regions, respectively. In § 7 we estimate the extinction to the Pa α -emitting regions. In § 8 we estimate the extended H α emission, and in § 9 we discuss the star formation rates of local LIRGs.

¹ Departamento de Astrofísica Molecular e Infrarroja, Instituto de Estructura de la Materia, CSIC, Serrano 121, 28006 Madrid, Spain; aalonso@damir.iem.csic.es.

² Steward Observatory, University of Arizona, 933 North Cherry Avenue, Tucson, AZ 85721.

³ Anglo-Australian Observatory, PO Box 296, Epping, NSW 1710, Australia.

TABLE 1
THE SAMPLE OF LOCAL UNIVERSE LIRGS

Galaxy Name (1)	IRAS Name (2)	v_{hel} (km s^{-1}) (3)	Distance (Mpc) (4)	$\log L_{\text{IR}}$ (L_{\odot}) (5)	Spectral Class (6)	References (7)	Morphology (8)
NGC 23.....	IRASF 00073+2538	4566	59.6	11.05	H II	1	paired with NGC 26
MCG +12-02-001.....	IRASF 00506+7248	4706	64.3	11.44	in group?
NGC 633.....	IRASF 01341-3735	5137	67.9	11.09:	H II	2, 3	paired with ESO 297-G012
UGC 1845.....	IRASF 02208+4744	4679	62.0	11.07	isolated
NGC 1614.....	IRASF 04315-0840	4746	62.6	11.60	H II	1, 2, 3	merger
UGC 3351.....	IRASF 05414+5840	4455	60.9	11.22	Sy2	4, 5	paired with UGC 3350
NGC 2369.....	IRASF 07160-6215	3237	44.0	11.10	isolated
NGC 2388.....	IRASF 07256+3355	4134	57.8	11.23:	H II	1	paired with NGC 2389
MCG +02-20-003.....	IRASF 07329+1149	4873	67.6	11.08:	in group
NGC 3110.....	IRASF 10015-0614	5034	73.5	11.31:	H II	2	paired with MCG -01-26-013
NGC 3256.....	IRASF 10257-4339	2814	35.4	11.56	H II	6	merger
NGC 3690/IC 694.....	IRASF 11257+5850	3121	47.7	11.88	Sy2-H II	7	close interacting pair
ESO 320-G030.....	IRASF 11506-3851	3232	37.7	11.10	H II	8	isolated
MCG -02-33-098E/W.....	IRASF 12596-1529	4773	72.5	11.11	H II (both)	1, 3	close interacting pair
IC 860.....	IRASF 13126+2453	3347	59.1	11.17:	H II	5	isolated
NGC 5135.....	IRASF 13229-2934	4112	52.2	11.17	Sy2	2,3	in group
NGC 5653.....	IRASF 14280+3126	3562	54.9	11.06	H II	1	isolated
NGC 5734.....	IRASF 14423-2039	4074	59.3	11.06:	NO	1	paired with NGC 5743
IC 4518E/W.....	IRASF 14544-4255	4715	69.9	11.13	Sy2 (W)	2	close interacting pair
Zw 049.057.....	IRASF 15107+0724	3897	59.1	11.27:	H II	1, 5	isolated
NGC 5936.....	IRASF 15276+1309	4004	60.8	11.07	H II	1	isolated
—.....	IRASF 17138-1017	5197	75.8	11.42	H II	2, 3	isolated?
IC 4687/IC 4686.....	IRASF 18093-5744	5200/4948	74.1	11.55:	H II (both)	3, 9	close interacting pair
IC 4734.....	IRASF 18341-5732	4680	68.6	11.30	H II/L	2	in group
NGC 6701.....	IRASF 18425+6036	3965	56.6	11.05	H II:	1	isolated
NGC 7130.....	IRASF 21453-3511	4842	66.0	11.35	L/Sy	1, 2	peculiar
IC 5179.....	IRASF 22132-3705	3422	46.7	11.16	H II	1	isolated
NGC 7469.....	IRASF 23007+0836	4892	65.2	11.59	Sy1	1	paired with IC 5283
NGC 7591.....	IRASF 23157+0618	4956	65.5	11.05	L	1	isolated
NGC 7771.....	IRASF 23488+1949	4277	57.1	11.34	H II	1	paired with NGC 7770

NOTES.—Col. (1): Galaxy name. Col. (2): *IRAS* denomination from Sanders et al. (2003). Col. (3): Heliocentric velocity from NED. Col. (4): Distance taken from Sanders et al. (2003). Col. (5): 8–1000 μm IR luminosity taken from Sanders et al. (2003), where colon (:) indicates large uncertainty (see Sanders et al. 2003 for details). NGC 633 was identified as the *IRAS* source in Sanders et al. (1995). Interacting pairs for which Surace et al. (2004) obtained *IRAS* fluxes for the individual components: NGC 633 $\log L_{\text{IR}} = 10.56$, and for NGC 2388, NGC 7469, and NGC 7771 with values of $\log L_{\text{IR}}$ similar to those given in Sanders et al. (2003). Col. (6): Nuclear activity class from spectroscopic data (Sy = Seyfert, L = LINER, H II = H II region-like, NO = no classification was possible, ... = no data available). Col. (7): References for the spectroscopic data. Col. (8): Morphological description.

REFERENCES.—(1) Veilleux et al. 1995; (2) Corbett et al. 2003; (3) Kewley et al. 2001; (4) Véron-Cetty & Véron 2001; (5) Baan et al. 1998; (6) Lipari et al. 2000; (7) García-Marín et al. 2006; the Sy2 classification is for B1 in NGC 3690; (8) van den Broek et al. 1991; (9) Sekiguchi & Wolstencroft 1992.

Our conclusions are given in § 10. Throughout this paper we use $H_0 = 75 \text{ km s}^{-1} \text{ Mpc}^{-1}$.

2. THE SAMPLE

We have selected a volume-limited sample of nearby LIRGs from the *IRAS* Revised Bright Galaxy Sample (RBGS; Sanders et al. 2003). The velocity range ($v_{\text{hel}} = 2750\text{--}5200 \text{ km s}^{-1}$) of the galaxies was chosen so that the Pa α emission line ($\lambda_{\text{rest}} = 1.876 \mu\text{m}$) falls within the *HST* NICMOS F190N narrowband filter. We required the logarithm of the total IR luminosity to be ≥ 11.05 and the galaxies to be at Galactic latitude $|b| > 10^\circ$. The sample is composed of 30 systems (34 individual galaxies) and contains 77% of the complete sample of systems within this velocity range in the RBGS.

The sample is presented in Table 1. The IR luminosities (and distances) of the systems are taken from the RBGS (Sanders et al. 2003), and are in the range $\log L_{\text{IR}} = 11.05\text{--}11.88 [L_{\odot}]$. Five of these systems (NGC 1614, NGC 3256, NGC 3690/IC 694, Zw 049.057, and NGC 7469) were part of the NICMOS guaranteed time observations (GTO; see Scoville et al. 2000; Alonso-Herrero et al. 2000, 2001, 2002), and one (NGC 5653) was part of the NICMOS Snapshot Survey of Nearby Galaxies (Böker

et al. 1999). The remaining 24 systems are new general observer (GO) observations obtained during *HST* Cycle 13.

In Table 1 we also list, if available, the nuclear activity class (H II, Seyfert, or LINER) obtained from spectroscopic observations in the literature (see Table 1 notes for references). The galaxies show a variety of morphologies and environments, including isolated systems, galaxies in groups, interacting galaxies, and advanced mergers. In the case of close interacting galaxies, the listed IR luminosities correspond to both galaxies in the system. Surace et al. (2004) presented high-resolution *IRAS* images for close interacting systems within the RBGS. Their work contains four systems in our sample for which the *IRAS* fluxes of the individual components of the pair are available, as listed in the notes to Table 1. There are four further systems for which Surace et al. (2004) could not obtain *IRAS* fluxes for the two individual components: MCG -02-33-098E/W, IC 4518E/W, IC 4686/IC 4687, and Arp 299. The components of Arp 299 have been amply studied in the mid-IR, and their contributions to the total IR luminosity of the system are well determined (see, e.g., Soifer et al. 2001).

For various reasons, nine galaxies that meet our selection criteria have not been imaged in Pa α : UGC 2982, CGCG 468-002,

NGC 23

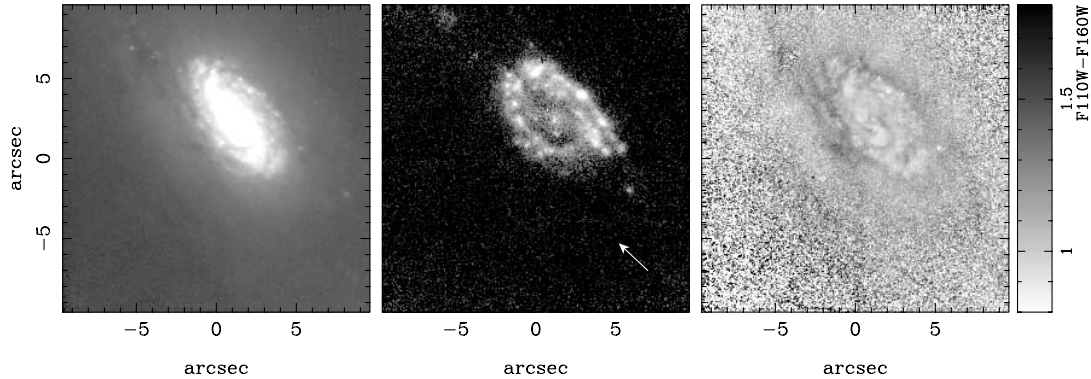


FIG. 1.1. NGC 23

FIG. SET 1.—*HST* NICMOS 1.1 μm continuum emission images (F110W filter; *left panels*), continuum-subtracted Pa α line emission images (F190N–F187N filters; *middle panels*), and $m_{\text{F110W}} - m_{\text{F160W}}$ color maps (*right panels*; the scale on the right hand side of the images is the $m_{\text{F110W}} - m_{\text{F160W}}$ color in magnitudes) for the galaxies in our sample observed during Cycle 13. The arrow indicates north, and east is in the counterclockwise direction. [See the electronic edition of the *Journal* for Figs. 1.2–1.26.]

ESO 264-G057, MCG –03-34-064, IC 4280, UGC 8739, ESO 221-G010, NGC 5990, and NGC 7679. We have examined these galaxies carefully to see if their properties depart from those in the observed sample. They do not. For example, the average logarithm of the luminosity of the observed galaxies is $\log L_{\text{IR}} = 11.25 [L_{\odot}]$, while for the unobserved ones it is $\log L_{\text{IR}} = 11.11 [L_{\odot}]$. The average redshift of the former group is 4317 km s^{-1} , and for the latter is 4722 km s^{-1} . The IR spectral shapes are generally similar, except that the observed sample contains both of the galaxies that *IRAS* did not detect at $12 \mu\text{m}$, IC 860 and Zw 049.057.

Within the errors, these galaxies all have approximately solar metallicity. Although this conclusion is expected, we were able to confirm it for all but three members of the sample (MCG +12-02-001, UGC 1845, and IC 860). We did so from measurements of $[\text{N II}]/\text{H}\alpha$ and $[\text{O III}]/\text{H}\beta$ from the literature, converted to $12 + \log(\text{O}/\text{H})$ according to the correlations found by Melbourne & Salzer (2002). For the first two exceptions, we could not find adequate data, while for IC 860 the emission-line equivalent width is very small, and the data in the literature are not consistent. For all the others, the computed metallicity is within a factor of 2 of solar. Given the approximate approach to the calculations, this factor is easily within the errors.

For our selected range of distance, the *IRAS* sample of LIRGs should be essentially complete (excluding regions of high-IR cirrus and those not surveyed). Our observed sample is 77% complete in terms of the *IRAS* sample, and the missing galaxies are very similar to those observed. We conclude that our results will be representative of local LIRGs in general.

3. *HST* NICMOS OBSERVATIONS

In this section we only describe the new *HST* NICMOS observations obtained in Cycle 13. We refer the reader to Scoville et al. (2000) and Alonso-Herrero et al. (2000, 2001, 2002) for details on the GTO observations, data reduction, and flux calibration of the data obtained prior to Cycle 13 (see § 2).

3.1. Data Reduction

The observations of the LIRGs were taken with the NIC2 camera (plate scale of $0.076'' \text{ pixel}^{-1}$) using the F110W and F160W broadband filters, and the F187N and F190N narrowband filters. At the distances of the LIRG sample, the F190N filter contains the Pa α emission line and the adjacent continuum

at $1.90 \mu\text{m}$. For continuum subtraction, we used the images taken through the F187N filter. The field of view (FOV) of the images is approximately $19''.5 \times 19''.5$, which for our sample covers the central 3.3–7.2 kpc of the galaxies. The observations were designed such that each galaxy could be observed within one *HST* orbit. The typical integration times were 250 s for each of the broadband filters and 900–950 s for each of the narrowband filters. For each filter the total integration time was split into three individual exposures with relative offsets of 5 pixels.

The images were reduced using the *HST* NICMOS pipeline routines, which involve subtraction of the first readout, dark current subtraction on a readout-by-readout basis, correction for linearity and cosmic-ray rejection, and flat fielding. For a given filter, the individual images were aligned using common features present in all three images and combined to construct a mosaic. The final F110W images, continuum-subtracted Pa α images, and F110W – F160W color maps are presented in Figure Set 1 for the new observations of galaxies in our sample.

The flux calibration of the images was performed using conversion factors given in the *HST* NICMOS handbook. We have also examined the near-IR continuum images and the $m_{\text{F110W}} - m_{\text{F160W}}$ color maps (Fig. Set 1) to look for the presence of nuclear point sources. When a nuclear point source was detected, we obtained photometry with a $1''$ diameter aperture (subtracting the underlying galaxy emission measured in an annulus around the point source) and performed an aperture correction (from the NICMOS handbook) to include all the flux from the point source. The typical photometry uncertainties associated with removing the underlying galaxy emission were 0.04–0.06 mag. If a nuclear point source was not detected, we measured the continuum emission using a similarly sized aperture but without removing the emission from the underlying galaxy. The results for the nuclei are presented in Table 2, and discussed in § 4.2.

3.2. Photometry of H II Regions

The continuum-subtracted Pa α line emission images were produced by subtracting the F187N images from the F190N images, both calibrated in Jy. Using the F190N filter, we estimate that for galaxies at $5000 \lesssim v \lesssim 5200 \text{ km s}^{-1}$ up to 20% (for the typical widths of hydrogen recombination lines of LIRGs not containing a type 1 AGN, see Goldader et al. 1997a) of the Pa α flux could be lost due to the observed wavelength of the emission line (see discussion in Alonso-Herrero et al. 2002).

TABLE 2
OBSERVED PHOTOMETRY OF THE NUCLEI OF LIRGS

Galaxy (1)	m_{F160W} (2)	$m_{F110W} - m_{F160W}$ (3)	f_{F187N}/f_{F160W} (4)	M_{F160W} (5)
Nuclear Point Sources				
NGC 23.....	13.26	1.07	0.99	-20.6
NGC 633.....	14.78	1.14	1.03	-19.4
MCG +12-02-001.....	13.61	1.37	1.15	-20.4
UGC 1845.....	12.41	1.48	1.21	-21.6
NGC 2388.....	13.07	1.26	1.13	-20.7
MCG -02-33-098W.....	14.26	1.22	1.19	-20.0
IC 860.....	14.43	1.54	1.25	-19.6
NGC 5135.....	14.46	1.45	1.54	-19.1
NGC 5734.....	13.51	1.11	0.98	-20.4
IC 4518W.....	14.40	1.95	1.74	-19.8
IC 4686.....	13.29	0.92	1.01	-21.1
NGC 6701.....	13.68	1.10	1.02	-20.1
IC 5179.....	14.00	1.32	1.17	-19.4
NGC 7771.....	14.99	1.67	1.32	-18.8
Nuclear Regions				
UGC 3351.....	13.97	1.93	1.30	-20.0
NGC 2369*.....	14.23	1.59	1.30	-19.0
MCG +02-20-003.....	13.94	1.54	1.29	-20.2
NGC 3110.....	14.19	1.19	1.11	-20.1
ESO 320-G030*.....	13.62	1.28	1.11	-19.3
MCG -02-33-098E.....	14.64	1.30	1.19	-19.7
IC 4518E.....	14.66	1.44	1.21	-19.6
IRAS 17138-1017*.....	14.74	1.87	1.38	-19.7
IC 4687.....	14.24	1.33	1.14	-20.1
IC 4734.....	13.27	1.43	1.19	-20.9
NGC 7130.....	13.56	0.95	1.11	-20.5
NGC 7591.....	13.49	1.43	1.21	-20.6

NOTES.—Col. (1): Galaxy name. Col. (2): Observed NICMOS F160W magnitude. Col. (3): Observed $m_{F110W} - m_{F160W}$ color. The typical color of an old stellar population is $m_{F110W} - m_{F160W} = 1.03$, based on the integrated spectrum of an elliptical galaxy using the filter transmissions and the quantum efficiency curves for the NICMOS filters. Col. (4): $1.87 \mu\text{m}$ to $1.60 \mu\text{m}$ continuum flux ratio. For the same elliptical galaxy as in col. (3), the $1.87 \mu\text{m}$ to $1.60 \mu\text{m}$ flux density ratio is $f_{F187N}/f_{F160W} \simeq 0.85$. Col. (5): Absolute NICMOS F160W magnitude. Asterisk (*) denotes not an obvious nucleus; the aperture was centered at the brightest F187N source. In the case of IRAS 17138-1017 this corresponds to the northern nucleus (see Zhou et al. 1993). In addition, near-IR nuclear point sources are present in NGC 7469 (Seyfert 1 nucleus; $M_{F160W} = -22.9$; Scoville et al. 2000), NGC 1614 ($M_{F160W} = -22.3$), NGC 3690 (B1: $M_{F160W} = -19.5$; B2: $M_{F160W} = -20.2$), NGC 5653 ($M_{F160W} = -20.8$), and NGC 3256 ($M_{F160W} = -20.2$).

We have used SExtractor (Bertin & Arnouts 1996) to analyze the properties of the individual H II regions detected in the Pa α images of our sample of galaxies. We have set the lower limit for the size of an H II region to 9 contiguous pixels. For the distances of the galaxies in our sample, this corresponds to minimum linear sizes (equivalent diameters) of between 44 and 96 pc. The detection threshold criterion for a pixel to be included as part of an H II region is to be above the background plus twice the rms noise of the background. SExtractor constructs a background image by a bicubic interpolation over areas of the background with a size specified by the user. These areas ought to be larger than the typical size of an H II region, but not so large as to smooth over local variations of the background. The main source of uncertainty in measuring the Pa α fluxes of the H II regions is the background removal. After modeling the background and H II regions, we output their positions and isophotal fluxes, errors, and areas after subtracting the global background from the observed Pa α flux.

The properties of the H II regions detected in the LIRGs are summarized in Table 3. We list the H α luminosity (the Pa α /H α ratio varies by about 10% for various conditions and under case B; we take a ratio of 8.6 from Hummer & Storey 1987) for the median H II region, the brightest H II region, and the average H α luminosity of the three brightest H II regions (first-ranked H II regions), as well as the ratio of the sum of the luminosities of the three brightest H II regions to the observed H α luminosity in H II regions, and the observed H α luminosity in H II regions. These properties are discussed in § 6.

4. NEAR-IR CONTINUUM PROPERTIES OF THE CENTRAL REGIONS OF LIRGS

4.1. Morphology

Morphological studies of complete samples of local ULIRGs have found that the great majority appear to be merging and/or disturbed systems (e.g., Murphy et al. 1996; Clements et al. 1996). At lower IR luminosities (the LIRG category), morphological studies have shown similarities with the ULIRG class, although the fraction of strongly interacting/disturbed systems appears to be smaller, approximately 50%–60% (Wu et al. 1998). However, these LIRG studies have often been conducted for incomplete samples or have been focused on the most luminous objects of this class (e.g., Wu et al. 1998; Arribas et al. 2004).

The present study extends the previous high-resolution near-IR morphological studies of LIRGs and ULIRGs (see Scoville et al. 2001; Bushouse et al. 2002) to a representative local sample in which most galaxies are at the lower luminosity end of the LIRG range. In our sample, approximately 50% of the systems are pairs, but only a small fraction are closely interacting/merging galaxies (see Table 1).

The most common continuum features in our sample are luminous star clusters and large-scale spiral arms. Two-armed spiral arm structures are also observed extending down to the center (inner kiloparsec scale, the so-called nuclear dusty spirals; see Martini et al. 2003). These spiral structures (both large- and small-scale) are also present in at least one galaxy member of close interacting systems or in mergers (NGC 1614, IC 694, and IC 4687), and pairs of galaxies. In closely interacting systems, a more perturbed central morphology would be expected (and is observed; see Scoville et al. 2000; Bushouse et al. 2002), although this depends on a number of factors, including the relative sizes and amount of gas present in the galaxies involved, and the stage of the interaction.

In highly inclined galaxies in our sample, dust lanes crossing the disks are common and present the reddest $m_{F110W} - m_{F160W}$ colors (see Fig. Set 1). If these dust lanes are hiding an old stellar population (see Table 2), the typical extinctions would be in excess of $A_V = 3-4$ mag, using the Rieke & Lebofsky (1985) extinction law.

The most “extreme” morphological features commonly observed in more IR luminous systems (see Scoville et al. 2000; Bushouse et al. 2002), such as double/multiple nuclei systems with a large number of bright star clusters near their centers and star-forming regions in the interface of interacting galaxies, are not very common in our sample of LIRGs. The most representative examples in this class are NGC 3690 (see Alonso-Herrero et al. 2000) and NGC 3256 (see Alonso-Herrero et al. 2002; Lipari et al. 2004). These two systems are among the most IR-luminous objects in our sample.

In terms of the central dust distribution, a few galaxies are dominated by nuclear extinction: IC 860, MCG -02-33-098E/W, IC 4518W, and IRAS 17138-1017, whereas in other galaxies the

TABLE 3
STATISTICS OF THE H II REGIONS IN THE CENTRAL REGIONS OF LIRGs

Galaxy (1)	Pa α Morphology (2)	$\log L(\text{H}\alpha)_{\text{median}}$ (ergs s $^{-1}$) (3)	$\log L(\text{H}\alpha)_{\text{br}}$ (ergs s $^{-1}$) (4)	$\log L(\text{H}\alpha)_3$ (ergs s $^{-1}$) (5)	$L(\text{H}\alpha)_3/L(\text{H}\alpha)_{\text{H II}}$ (6)	$L(\text{H}\alpha)_{\text{H II}}$ ($\times 10^{40}$ ergs s $^{-1}$) (7)
Cycle 13						
NGC 23.....	R	39.53	40.94	40.90	0.24	99.6
MCG +12-02-001.....	M	39.50	41.96	41.60	0.61	199.4
NGC 633.....	R	39.16	41.17	40.88	0.63	36.5
UGC 1845.....	M	39.32	41.23	41.03	0.39	81.7
UGC 3351.....	E	39.20	40.71	40.60	0.35	34.1
NGC 2369.....	E	38.96	40.87	40.80	0.39	48.6
NGC 2388.....	E	39.33	41.66	41.26	0.67	81.4
MCG +02-20-003.....	C	39.25	41.31	40.96	0.69	39.4
NGC 3110.....	S	39.60	40.90	40.82	0.30	64.8
ESO 320-G030.....	R	39.47	40.31	40.28	0.13	43.6
MCG -02-33-098.....	C	...	41.76	...	0.95	101.6
IC 860.....	C	...	40.13	...	0.90	1.9
NGC 5135.....	M	39.49	41.05	41.00	0.36	83.1
NGC 5734.....	S	39.19	40.52	40.28	0.19	29.6
IC 4518W.....	C	39.52	41.28	41.16	0.69	62.4
IC 4518E.....	E	...	40.21	40.16	0.40	10.8
NGC 5936.....	M, S	39.23	41.24	41.05	0.68	50.3
IRAS 17138-1017.....	M	39.63	41.24	41.10	0.38	99.9
IC 4687.....	S	39.76	41.42	41.22	0.24	211.0
IC 4686.....	C	...	41.63	...	0.91	82.1
IC 4734.....	C, S	39.20	41.02	40.99	0.54	54.3
NGC 6701.....	M	39.64	40.91	40.78	0.40	45.1
NGC 7130.....	S	39.34	41.69	41.30	0.74	80.4
IC 5179.....	S	39.24	41.18	40.81	0.39	49.0
NGC 7591.....	C, S	39.24	41.06	40.80	0.85	22.1
NGC 7771.....	R, E, S	39.62	41.05	40.90	0.31	76.0
Prior to Cycle 13						
NGC 1614.....	R	39.88	40.99	40.98	0.08	380.2
NGC 3256.....	S	39.47	41.49	41.20	0.40	120.2
NGC 3690.....	S	39.83	41.54	41.44	0.44	186.2
IC 694.....	S	39.67	41.82	41.40	0.66	114.8
NGC 5653.....	S	39.62	41.15	40.87	0.23	97.7
Zw 049.057.....	E	...	41.32	...	≈ 1	20.9

NOTES.— Col. (1): Galaxy name. Col. (2): Pa α morphology described in § 5: C = compact emission, M = nuclear minispiral, R = ring of star formation, S = H II regions in spiral arms, E = edge-on galaxy. Col. (3): H α luminosity of the median H II region for galaxies with more than 20 H II regions detected. The typical standard deviations from the mean value of the distribution of H α luminosities of the H II regions detected is 0.4–0.6 dex for a given galaxy. Col. (4): H α luminosity of the brightest H II region. Col. (5): Average H α luminosity of the brightest three (first-ranked) H II regions. The typical uncertainties for the SExtractor fluxes for the brightest and first-ranked H II regions are 1%–2%. Col. (6): Ratio of the sum of the H α luminosities of the brightest three H II regions to the H α luminosity in H II regions. Col. (7): Observed H α luminosity in H II regions in the central regions. The top part of the table lists galaxies observed in Cycle 13; below are given the galaxies observed prior to Cycle 13 and presented in Alonso-Herrero et al. (2002), recomputed for the distances used in this paper.

regions of the largest extinction do not coincide with the nucleus of the galaxy (e.g., NGC 3110, NGC 5734). In the cases of galaxies with nuclear rings of star formation (see § 5.3), the H II regions are interleaved with the dust features, or the color maps trace a ring of extinction just outside the ring of H II regions (e.g., NGC 23 and NGC 1614; see Alonso-Herrero et al. 2001).

4.2. Nuclei of Galaxies

Scoville et al. (2000) and Bushouse et al. (2002) found near-IR pointlike nuclear sources in approximately 30%–50% of the galaxies in their samples of IR-bright galaxies (i.e., some LIRGs but mostly ULIRGs). Scoville et al. (2000) established that in about one-third of their sample these nuclear point sources dominate the near-IR emission at 2.2 μm . These bright nuclear point sources are more prevalent in LIRGs and ULIRGs with Seyfert or quasar activity. This is not surprising, as bright near-IR nu-

clear point sources are common in nearby Seyfert 1 galaxies, and are present in about 50% of nearby Seyfert 2 galaxies (see Quillen et al. 2001). However, galaxies with no evidence of AGN activity can also show nuclear point sources, believed to be nuclear star clusters. The typical luminosities of the nuclear star clusters in late-type spiral galaxies are in the range 10^6 – $10^7 L_{\odot}$ (Böker et al. 2004 and references therein), similar to those of the so-called super star clusters, and more luminous galaxies tend to harbor more luminous nuclear clusters.

We have found that approximately 70% of the galaxies in our sample (including the galaxies observed prior to Cycle 13) show nuclear point sources, with observed (not corrected for extinction) absolute H -band magnitudes ranging from $M_{\text{F160W}} = -22.9$ (for the bright Seyfert 1 nucleus in NGC 7469) to $M_{\text{F160W}} = -18.8$, with an average value of $M_{\text{F160W}} = -20.3$ (see Table 2). The observed absolute H -band magnitudes for the resolved

central regions (for sizes 170–370 pc, depending on the distance) are similar to those of the nuclear point sources. In general, the observed range of F160W absolute magnitudes (Table 2) does not allow us to discriminate between AGNs and star clusters. We also find that these point sources do not dominate the near-IR emission except in some of the most IR-luminous galaxies (e.g., at 2.2 μm the Seyfert 1 nucleus of NGC 7469 [see Scoville et al. 2000], and component B1 in Arp 299 [see Alonso-Herrero et al. 2000]), or in the case of the compact galaxy IC 4686.

The majority of the nuclei display redder colors (see Table 2) than those typical of an old stellar population, implying extinctions of a few magnitudes (or higher if the stellar population is young; see § 7.2) for a simple dust screen model. Scoville et al. (2000) found values of the nuclear $m_{F110W} - m_{F160W}$ colors of between 1 and 2 for both LIRGs and ULIRGs in their sample, similar to the colors observed in our sample. Scoville et al. (2000) also found that the $m_{F160W} - m_{F222M}$ colors tend to be redder for the ULIRGs than for the less luminous LIRGs in their sample. We do not see any clear evidence for this behavior, although our sample, unlike that of Scoville et al. (2000), does not contain examples of the most extreme cases of ULIRGs hosting quasars, known to present very red near-IR colors.

5. MORPHOLOGY OF THE Pa α LINE EMISSION OF THE CENTRAL REGIONS OF LIRGs

The *HST* NICMOS Pa α observations presented in this study afford us the best opportunity to study the H II region emission with spatial resolutions of 25–50 pc in a sample of local LIRGs. The advantage of the Pa α observations compared to optical H α observations is that the extinction is reduced by a factor of ~ 5 ($A_{\text{Pa}\alpha} \simeq 0.18A_{\text{H}\alpha}$, using the Rieke & Lebofsky 1985 extinction law). In very dusty systems, such as those under consideration here, high spatial resolution mid-IR imaging has shown the location (nuclear regions) and extent (approximately on scales of 1 kpc or less) of the current dusty star formation (Soifer et al. 2001). It is of interest to determine whether the Pa α emission is able to penetrate the high column densities traced by the mid-IR emission.

We have grouped the main morphological Pa α features present in the LIRG sample (see middle panels of Fig. Set 1) into five categories. We note that some galaxies show morphologies that place them in more than one category (see Table 3).

5.1. Compact ($\lesssim 1$ kpc) Nuclear Pa α Emission

The Pa α morphology appears to be dominated by the nuclear emission (see Table 3 for the galaxies in this class) with sizes of $\lesssim 1$ kpc, although fainter H II regions are also present outside of the nuclear regions. In some cases this compact emission appears to be related to the presence of an AGN (see Table 1 and § 9.2.2). The average observed H α surface brightnesses (derived from Pa α) are among the highest in our sample of galaxies, 5–10 $\times 10^{41}$ ergs s $^{-1}$ kpc $^{-2}$.

5.2. Nuclear Minispiral (Inner 1–2 kpc) Pa α Emission

In these cases we observe bright H II regions as well as bright star clusters along a nuclear minispiral structure (see Table 3) also detected in continuum light (see § 4.1, and Martini et al. 2003). The typical observed H α surface brightnesses are similar to those of the galaxies with compact Pa α emission.

5.3. Nuclear Star-forming Rings

The nuclear rings in our sample of LIRGs (Table 3) have diameters ranging from 0.7 to 2 kpc, show resolved H II regions

within them, and dominate the central Pa α emission in these galaxies. Fainter H II regions are also present in the spiral arms in these systems. The typical observed (not corrected for extinction) H α surface brightnesses in the H II regions are 2–4 $\times 10^{41}$ ergs s $^{-1}$ kpc $^{-2}$, although the ring of star formation in NGC 1614 has an H α surface brightness of $\simeq 60 \times 10^{41}$ ergs s $^{-1}$ kpc $^{-2}$. All these nuclear rings of star formation except the one in ESO 320-G030 are located in interacting galaxies.

5.4. Large-scale (Several kpc) Pa α Emission with H II Regions Located in the Spiral Arms

In this category we find LIRGs with H II regions located over several kpc along the spiral arms of the galaxy (see Table 3). Although our images only cover the central $\simeq 3.3$ –7.2 kpc, several of these galaxies are known to show H α emission over larger scales (see § 8, and Lehnert & Heckman 1995; Dopita et al. 2002; Hattori et al. 2004). The observed H α surface brightnesses in H II regions are about 1 order of magnitude fainter than those of galaxies with compact Pa α emission.

In some cases the nuclear compact Pa α emission is bright and can make a significant contribution to the total H II region emission, for instance in IC 694 and NGC 3690 (see Alonso-Herrero et al. 2000) and NGC 3256 (see Alonso-Herrero et al. 2002). In this class we also find examples of galaxies without bright nuclear emission or large numbers of bright H II regions in the spiral arms (IC 4687), and even galaxies whose Pa α emission is dominated by one or a few bright extranuclear H II regions, such as NGC 5653 (see Böker et al. 1999; Alonso-Herrero et al. 2002) and NGC 5734.

5.5. Large-scale Pa α Emission in Highly Inclined Dusty Systems

In these cases (see Table 3) the Pa α emission traces the least obscured H II regions along the disk of the galaxies over scales of a few kpc (3.3–7.2 kpc, at least; see § 8). This category is similar to that discussed in § 5.4, but for galaxies viewed edge-on. These galaxies tend to show the reddest $m_{F110W} - m_{F160W}$ central colors over the extent of the Pa α emission (see right panels of Fig. Set 1).

Summarizing, in half the galaxies in our sample, most of the Pa α emission is more compact than the continuum near-IR emission, and is located in the inner 1–2 kpc of the galaxies, as also shown by mid-IR observations (Soifer et al. 2001) of a few bright LIRGs. In a few cases the nuclear emission even dominates the total Pa α emission (see further discussion in § 8). However, in the other half of our sample the Pa α emission is extended on scales larger than a few kpc (as discussed in §§ 5.4 and 5.5).

6. PROPERTIES OF THE H II REGIONS IN LIRGs

Alonso-Herrero et al. (2002) showed for a sample of seven⁴ LIRGs that these galaxies contained a significant number of exceptionally bright H II regions (based on the median values of the H II region luminosity distribution), with H α luminosities comparable to that of the giant H II region 30 Doradus ($\log L(\text{H}\alpha) = 39.70$ [ergs s $^{-1}$]; Kennicutt et al. 1989). This small sample was, however, heavily biased toward the most IR-luminous objects in the LIRG class. Table 3 summarizes the statistical properties of the H II regions detected in our sample of LIRGs.

Confirming the results of Alonso-Herrero et al. (2002), the LIRGs in our sample with the highest IR and observed H α

⁴ Two galaxies in their sample, VV 114 and NGC 6240, are at $v > 5200$ km s $^{-1}$, and thus are not included in our sample.

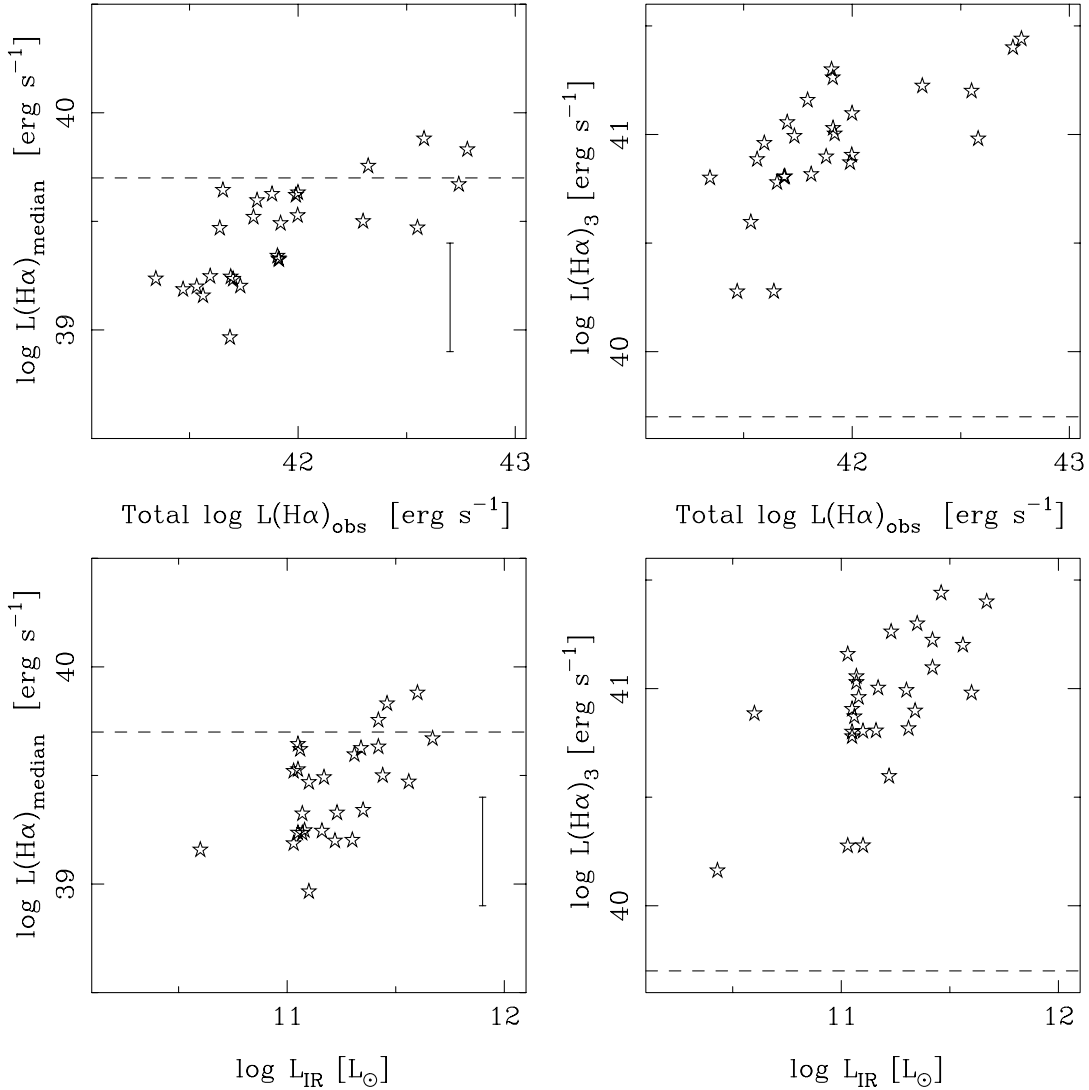


FIG. 2.—*Left panels:* H α luminosity of the median H II region as a function of the IR luminosity (*bottom*) and total observed (not corrected for extinction) H α luminosity of the galaxy (*top*) in H II regions in the central regions. The horizontal dashed line shows the H α luminosity of 30 Doradus in the LMC, the prototypical giant H II region. The error bar indicates the typical standard deviation from the mean value of the distribution of H II region H α luminosities of a given galaxy. *Right panels:* Average H α luminosity of the three brightest (first-ranked) H II regions as a function of the IR luminosity (*bottom*) and total observed (not corrected for extinction) H α luminosity of the galaxy (*top*).

luminosities have median H II regions with H α luminosities comparable to or brighter than the giant H II region 30 Dor (Table 3, and left panels of Fig. 2). Approximately 50% of our volume-limited sample of LIRGs have $\log L(\text{H}\alpha)_{\text{median}} > 39.5$ [ergs s $^{-1}$], significantly higher (about 1 order of magnitude) than the median H II regions of normal galaxies in the Virgo Cluster observed with similar spatial resolutions (see Alonso-Herrero & Knapen 2001).

The first-ranked (the brightest three) H II regions are usually coincident with the nuclei of the galaxies, although with notable exceptions, e.g., NGC 5653, NGC 5734, and IC 4687, as well as those galaxies with nuclear rings of star formation (see § 5.3). The average H α luminosities of the first-ranked H II regions are between 1 and 2 orders of magnitude brighter than the median H II regions, and are well above that of 30 Dor (Table 3). The contribution of the first-ranked H II regions to the total observed H α luminosity in H II regions in the central regions is given in Table 3. Not surprisingly, this contribution is highest for the galaxies with compact Pa α emission, where these regions also tend to coincide with or are near the nucleus of the galaxy.

There is a good correlation between the H α luminosity of the median H II regions and the IR and total observed H α luminosity of the system (left panels of Fig. 2). These correlations appear to be linear. We also show in these figures the typical standard deviation from the mean value of the distribution of H α luminosities of the detected H II regions for a given galaxy, an indication of the width of the distribution. Similarly, there is a good relation between the luminosity of the first-ranked regions and the IR and the total H α luminosity in H II regions (right panels of Fig. 2). The uncertainties for the SExtractor H α fluxes of the first-ranked H II regions (1%–2%) plus those of the distance determinations ($\sim 10\%$) of the galaxies do not account for the dispersion in H α luminosity of the first-ranked (and also median) H II regions for a given IR luminosity. This dispersion is probably due to resolution effects, as the distances of our galaxies span a factor of 2.

7. EXTINCTION CORRECTION OF Pa α MEASUREMENTS

We now prepare to compare the star formation rates (SFR) derived from the IR luminosity and from the number of ionizing

TABLE 4
Pa α AND H α FLUXES AND EXTINCTIONS

Galaxy (1)	Aperture (2)	$f(\text{H}\alpha)$ (ergs cm $^{-2}$ s $^{-1}$) (3)	$f(\text{Pa}\alpha)$ (ergs cm $^{-2}$ s $^{-1}$) (4)	A_V (mag) (5)	A_V (Veilleux) (mag) (6)
NGC 23.....	2'' \times 7'' (E-W)	2.5 \times 10 $^{-13}$	7.64 \times 10 $^{-14}$	1.7 \pm 0.4	2.3
NGC 3110.....	2'' \times 6'' (E-W)	*7.2 \times 10 $^{-14}$	4.64 \times 10 $^{-14}$	3.1 \pm 0.4	2.8
MCG -02-33-098E.....	2'' \times 6'' (N-S)	*3.0 \times 10 $^{-14}$	7.22 \times 10 $^{-14}$	5.5 \pm 0.4	4.5
MCG -02-33-098W.....	2'' \times 6'' (N-S)	*4.4 \times 10 $^{-14}$	1.05 \times 10 $^{-13}$	5.5 \pm 0.4	2.4
NGC 5734.....	2'' \times 7'' (E-W)	2.8 \times 10 $^{-14}$	3.48 \times 10 $^{-14}$	4.3 \pm 0.4	3.6
NGC 5936.....	2'' \times 7'' (E-W)	8.9 \times 10 $^{-14}$	1.11 \times 10 $^{-13}$	4.3 \pm 0.4	4.7
NGC 6701.....	1''.5 \times 7'' (E-W)	1.0 \times 10 $^{-13}$	6.32 \times 10 $^{-14}$	3.1 \pm 0.4	3.9
NGC 7130.....	1''.5 \times 6'' (E-W)	2.1 \times 10 $^{-13}$	1.10 \times 10 $^{-13}$	2.7 \pm 0.4	3.3
IC 5179.....	2'' \times 9'' (E-W)	4.4 \times 10 $^{-14}$	8.69 \times 10 $^{-14}$	5.1 \pm 0.4	3.7
NGC 7591.....	1''.5 \times 6'' (E-W)	2.4 \times 10 $^{-14}$	4.42 \times 10 $^{-14}$	5.0 \pm 0.4	4.3
NGC 7771.....	1''.5 \times 7'' (E-W)	5.9 \times 10 $^{-14}$	8.28 \times 10 $^{-14}$	4.5 \pm 0.4	6.3

NOTES.—Col. (1): Galaxy name. Col. (2): Extraction aperture of the optical spectroscopy. Col. (3): Observed H α flux from Veilleux et al. (1995). Asterisk (*) next to the H α fluxes indicates that the optical spectra were obtained under nonphotometric conditions (Kim et al. 1995). Col. (4): Observed Pa α flux for the same aperture. Col. (5): Spectroscopic extinction derived from the H α and Pa α fluxes. The errors are computed for a 15% uncertainty in the Pa α emission line flux measurements. Col. (6): Spectroscopic extinction derived from H α and H β by Veilleux et al. (1995) for the same extraction apertures.

photons (N_{Ly} ; see § 9). To do so, we must correct the observed hydrogen recombination line emission for extinction (see discussion in Kennicutt 1998). Since the mid-IR emission of (some) LIRGs is predominantly produced in nuclear starbursts with sizes of $\lesssim 1$ –2 kpc (see, e.g., Wynn-Williams & Becklin 1993; Miles et al. 1996; Keto et al. 1997; Soifer et al. 2001), there must be large concentrations of dust in their nuclear regions.

By far the largest uncertainty in determining the extinction comes from the unknown distribution of dust within the source. The color maps (Fig. Set 1) of most LIRGs in our sample show complicated dust features in their centers. In the cases of the deeply embedded star-forming regions, common in LIRGs and ULIRGs, a simple foreground dust screen model may not provide a good fit to the star-forming properties (e.g., see Genzel et al. 1995, 1998; Satyapal et al. 1999), and a model in which stars and dust are mixed will be more realistic (Witt & Gordon 2000). Moreover, the simple model of a foreground dust screen only provides a lower limit to the true obscuration, and in cases of high optical depths both models will only measure the obscuration to the material less affected by extinction (Goldader et al. 1997a). Because of this, in very dusty systems there is a tendency for the derived extinction to increase as longer wavelengths are used (see, e.g., McLeod et al. 1993; Genzel et al. 1998). Finally, there is the issue of whether the extinction to the stars is the same as the extinction to the gas. Calzetti et al. (1994) found that in general the extinction to the gas (ionized by the young stars) is twice that of the continuum (mostly produced by old stars), implying that the youngest ionizing stars are located in dustier regions than occupied by the cold stellar population. The lack of correspondence between gas emission and continuum emission generally observed in LIRGs (Fig. Set 1) suggests that this may also be the case for them.

7.1. Extinction to the Gas

Kim et al. (1995) and Veilleux et al. (1995), and Goldader et al. (1997a, 1997b) presented the most comprehensive optical and near-IR long-slit spectroscopic surveys, respectively, of the central regions of LIRGs. We have a number of galaxies in common with these studies for which we can estimate the extinction to the gas. We have simulated the sizes and orientations of the slits used by Kim et al. (1995) and Goldader et al. (1997a) to

measure the Pa α fluxes and compared them with their H α and Br γ measurements, respectively. We have then estimated the extinction to the gas using the Rieke & Lebofsky (1985) extinction law and a foreground dust screen model. In addition, for NGC 3256 we have used the Br γ fluxes of Doyon et al. (1994).

The results are presented in Tables 4 and 5. Table 4 also lists the A_V derived from H β and H α by Veilleux et al. (1995), which are generally similar to or slightly smaller than the A_V obtained from H α and Pa α . The extinctions derived using the longest wavelength emission lines (Table 5) tend to be higher for the few galaxies in common with H α and Pa α measurements. The average extinctions obtained from H α and Pa α over regions with typical sizes of 0.5 kpc \times 1.5 kpc are not too different from the A_V (derived using the same emission lines) of individual H II regions in spiral galaxies and starburst galaxies (see, e.g., Quillen & Yukita 2001; Maoz et al. 2001; Scoville et al. 2001; Calzetti et al. 2005).

7.2. Extinction to the Stars

We can alternatively use the observed near-IR colors to estimate the extinction to the young stars responsible for ionizing the H II regions. The near-IR colors in general present a smaller dependence on the age of the stellar population than the optical colors. However, there is a weak dependence, in particular for the youngest stellar populations responsible for ionizing the H II regions. Alonso-Herrero et al. (2002) found, for a small sample of LIRGs, that most young star-forming regions (with Pa α emission) in LIRGs have ages of $\simeq 1$ –9 Myr (depending on the type of star formation assumed).

Using the typical near-IR colors of a young ionizing stellar population predicted by the Rieke et al. (1993) models, and the observed F110W–F160W color maps (right panels of Fig. Set 1), we have derived two-dimensional extinction (referred to as photometric A_V) maps. The uncertainties of the extinction maps are given by the range of possible ages of the Pa α -emitting regions. The photometric A_V maps are only applicable to continuum regions with Pa α flux emission. For each galaxy, the extinction-corrected Pa α maps were constructed using the A_V maps and the observed Pa α images. To estimate the observed and extinction-corrected Pa α fluxes, we only added those pixels above the threshold used for estimating the fluxes of H II regions in § 6. An

TABLE 5
Pa α AND Br γ FLUXES AND EXTINCTIONS

Galaxy (1)	Aperture (2)	$f(\text{Br}\gamma)$ (ergs cm $^{-2}$ s $^{-1}$) (3)	$f(\text{Pa}\alpha)$ (ergs cm $^{-2}$ s $^{-1}$) (4)	A_V (mag) (5)
NGC 2388.....	3'' \times 9'' (E-W)	26.8×10^{-15}	2.02×10^{-13}	13 ± 5
NGC 3110.....	3'' \times 9'' (E-W)	6.0×10^{-15}	0.68×10^{-13}	2 ± 5
NGC 3256-nucleus.....	3''5 \times 3''5	54.0×10^{-15}	5.37×10^{-13}	6 ± 3
NGC 3256-5'' S.....	3''5 \times 3''5	15.0×10^{-15}	1.15×10^{-13}	15 ± 5
NGC 3256-5'' E.....	3''5 \times 3''5	17.0×10^{-15}
NGC 5135.....	3'' \times 12'' (E-W)	16.5×10^{-15}	1.95×10^{-13}	0.5 ± 5
IRAS 17138–1017.....	3'' \times 9'' (N-S)	22.4×10^{-15}	1.62×10^{-13}	14 ± 5
NGC 7130.....	1''5 \times 4''5 (E-W)	10.2×10^{-15}	1.00×10^{-13}	7 ± 5

NOTES.— Col. (1): Galaxy name. The two other galaxies in common with Goldader et al. (1997a) are NGC 1614, analyzed in Alonso-Herrero et al. (2001), and NGC 7469, for which the spectroscopic data includes the Seyfert 1 nucleus. Col. (2): Extraction aperture. Col. (3): Observed Br γ flux from Goldader et al. (1997a) for all galaxies except for NGC 3256, for which the data are from Doyon et al. (1994). For NGC 3256, the 5'' to the south location coincides with the secondary nucleus of the galaxy, and the 5'' to the east location, an H II region, is not fully covered by our Pa α image. Col. (4): Observed Pa α flux for the same aperture. Col. (5): Derived spectroscopic extinction. The errors are computed for a 15% uncertainty in the Pa α emission line flux measurements.

TABLE 6
PHOTOMETRIC EXTINCTIONS, EXTINCTION-CORRECTED
Pa α LUMINOSITIES, AND SFRs

Galaxy (1)	Phot A_V (mag) (2)	$\log L(\text{Pa}\alpha)_{\text{corr}}$ (ergs s $^{-1}$) (3)	$\log \text{SFR IR}/N_{\text{Ly}}$ (4)
NGC 23.....	$2.7^{+1.1}_{-0.8}$	41.32	0.14 (–0.01)
MCG +12-02-001.....	$4.5^{+1.0}_{-0.8}$	41.67	0.17
NGC 633.....	$2.6^{+1.0}_{-0.8}$	40.91	0.10
UGC 1845.....	$4.6^{+1.1}_{-0.8}$	41.33	0.14
UGC 3351.....	$5.9^{+1.0}_{-0.8}$	41.25	0.38 (0.23)
NGC 2369.....	$4.8^{+1.1}_{-0.9}$	41.16	0.34
NGC 2388.....	$3.5^{+1.1}_{-0.8}$	41.29	0.35
MCG +02-20-003.....	$3.3^{+1.0}_{-0.8}$	41.16	0.33
NGC 3110.....	$3.3^{+1.1}_{-0.8}$	41.26	0.45 (0.15)
ESO 320-G030.....	$3.3^{+1.1}_{-0.8}$	40.97	0.53
MCG–02-33-098.....	$3.3^{+1.1}_{-0.8}$	41.32	0.20
IC 860.....	$3.2^{+0.8}_{-0.7}$	39.86	1.72
NGC 5135.....	$3.3^{+1.1}_{-0.9}$	41.26	0.32
NGC 5734.....	$3.1^{+1.2}_{-0.9}$	41.05	0.39
IC 4518W.....	$4.1^{+0.8}_{-0.6}$	41.27	0.17
IC 4518E.....	$4.6^{+1.2}_{-0.9}$	40.72	0.12
NGC 5936.....	$3.7^{+1.3}_{-0.9}$	41.20	0.27
IRAS 17138–1017.....	$5.1^{+0.7}_{-0.8}$	41.48	0.34
IC 4687.....	$3.1^{+1.2}_{-0.9}$	41.63	0.19
IC 4686.....	$2.2^{+1.0}_{-0.7}$	41.21	0.15
IC 4734.....	$3.9^{+1.2}_{-0.9}$	41.19	0.52
NGC 6701.....	$3.0^{+1.1}_{-0.9}$	41.04	0.42 (0.27)
NGC 7130.....	$2.9^{+1.2}_{-0.8}$	41.30	0.45
IC 5179.....	$3.3^{+0.2}_{-0.8}$	41.22	0.35 (0.13)
NGC 7591.....	$4.1^{+1.2}_{-0.9}$	41.09	0.36
NGC 7771.....	$4.1^{+1.2}_{-0.9}$	41.36	0.39 (0.04)

NOTES.— Col. (1): Galaxy name. Col. (2): Average photometric extinction A_V over the Pa α -emitting region derived from the observed $m_{\text{F110W}} - m_{\text{F160W}}$ colors (see § 7.2). The uncertainties of phot A_V are for the possible range of ages of the Pa α -emitting regions (4 and 9 Myr) using the Rieke et al. (1993) models for a Gaussian burst with FWHM = 5 Myr (see Alonso-Herrero et al. 2002 for details). We also list the Pa α luminosities over the NICMOS FOV corrected for extinction, and uncertainties. Col. (3): Pa α luminosity corrected for extinction. Col. (4): log of the ratio between the IR and corrected for extinction N_{Ly} SFRs calculated using the prescriptions of Kennicutt (1998). In parentheses we give the values corrected for extended emission (§ 8, and Table 7).

estimate of the background is obtained from those pixels below the threshold value. We note that in computing the observed Pa α fluxes in this fashion, we are including more pixels than when measuring H II region fluxes with SExtractor (§ 3.2), as we are not imposing a criterion for defining the size of the emitting regions. The typical uncertainties for the summed Pa α fluxes are $\approx 30\%$, depending on the threshold value used for adding up the emission. The average photometric extinctions over the Pa α -emitting regions for our sample of galaxies are given in column (2) of Table 6.

A comparison with the spectroscopic extinctions in Tables 4 and 5 shows that the photometric extinctions are comparable to or slightly smaller than the extinctions to the gas for the galaxies in common. However, in most cases, the photometric extinctions are derived for larger areas than the regions covered by the spectroscopic observations. Since there is evidence that the extinction in spiral galaxies tends to decrease with distance from the galaxy center (Calzetti et al. 2005), the average photometric extinction measured over larger regions will tend to be smaller than the spectroscopic values. We also find that the highest values of the average photometric extinction over the Pa α -emitting regions tend to occur in those galaxies with the most compact (≈ 1 kpc) Pa α -emitting regions (e.g., MCG +12-02-001) or in the edge-on systems (e.g., NGC 2369, UGC 3351).

8. LARGE-SCALE EMISSION

As we saw in § 5, about half of the galaxies in our sample show extended Pa α emission covering the entire FOV of the NICMOS observations. Before we compare the Pa α (or H α) and IR luminosities, we need to assess the importance of the H II region and diffuse emission at large galactocentric distances, especially for the nearest examples in our sample. Hattori et al. (2004) for their sample of 60 μm flux-limited LIRGs, which includes some of the galaxies in our sample, have found that the star formation activity is dominated by emission extending over several kpc. We have obtained the H α images from Hattori et al. (2004) for the galaxies in common with our work, and measured the H α fluxes within the NICMOS FOV and the total extent of the galaxy. As can be seen from Table 7, the contribution from the large-scale H α emission can be as high as 50% in some galaxies. We have eight further galaxies in common with the sample of Dopita et al. (2002). From inspection of their H α images, which

TABLE 7
LARGE-SCALE EMISSION

Galaxy (1)	H α Diameter (arcsec) (2)	$f_{\text{NIC2 FOV}}/f_{\text{tot}}$	
		H α (3)	24 μm (4)
NGC 23.....	55	0.70	0.83
UGC 3351.....	0.73
NGC 3110.....	76	0.50	0.63
NGC 6701.....	0.73
IC 5179.....	0.61
NGC 7771.....	93	0.44	0.55

NOTES.— Col. (1): Galaxy. Col. (2): Diameter used to measure the total H α emission. Col. (3): Ratio of the observed H α emission over the NICMOS NIC2 FOV ($\sim 20'' \times 20''$) and the total observed H α emission using the images of Hattori et al. (2004). Col. (4): Ratio of the *Spitzer* MIPS 24 μm emission over the NICMOS FOV and the entire galaxy.

comprise the entire systems, we infer that the NICMOS Pa α images include most of the emission of NGC 633, MCG –02-33-098E/W, IC 4518E/W, NGC 5734, and IC 4686/IC 4687.

The H α images of IC 4734 and NGC 7130 (Dopita et al. 2002), as well as of IC 5179 (Lehnert & Heckman 1995) and NGC 6701 (Márquez et al. 1996) show H II region and diffuse H α emission over scales larger than the FOV of the Pa α images, and thus our extinction-corrected Pa α luminosities are lower limits to the total emission. If the average extinction of H II regions decreases for increasing galactocentric distances (Calzetti et al. 2005), as in spiral galaxies, the contributions from the large-scale component not covered by the NICMOS images derived from the H α images will be upper limits.

We have retrieved the available MIPS 24 μm images from the *Spitzer* archive and simulated the NICMOS FOV to estimate the contribution from the large-scale emission. At 24 μm the NICMOS FOV ($\sim 20'' \times 20''$) covers most of the emission (>85%) for the majority of the galaxies of the sample, except for those listed in Table 7. For those galaxies with available H α imaging, the agreement on the fraction of extended emission derived from the 24 μm imaging is reasonably good. We conclude that, with a few exceptions, the Pa α detected by NICMOS is representative of the totals for our sample of galaxies.

9. STAR FORMATION RATES OF LIRGs

Both the IR emission and N_{Ly} are good tracers of the massive SFR in galaxies. The N_{Ly} is usually derived from hydrogen recombination lines, and has the advantage that it traces the current massive SFR, almost independently of the previous star formation history of the galaxy (Kennicutt 1998). The main disadvantage in deriving SFRs from N_{Ly} is determining A_V and the fraction of escaping photons from H II regions. The former problem can be alleviated by using near-IR, mid-IR, and radio recombination lines (e.g., H92 α ; see Zhao et al. 1997; Roy et al. 2005). The issue of the fraction of escaping photons is still uncertain and is not considered here, but it has been addressed both observationally (Beckman et al. 2000) and theoretically (Bland-Hawthorn & Maloney 1999).

The IR luminosity of a starburst galaxy is due to UV emission (produced mainly by the young stellar population) absorbed by dust and re-emitted in the thermal IR. As discussed by Kennicutt (1998), the efficacy of the IR luminosity as a tracer of the SFR depends on the contribution of the young stars to the heating of the dust, and requires that all the UV light from massive stars be absorbed by the dust (i.e., $A_V > 1$ mag; see also Calzetti et al.

2005). In the presence of high dust opacities, as in LIRGs, the IR luminosity dominates the bolometric luminosity of the system and is the ultimate tracer of the SFR, but with a somewhat ill-determined timescale.

9.1. Comparison between the Mid-IR and IR Luminosities and the Extinction-corrected Pa α Luminosities

The mid-IR luminosities are routinely used to estimate the total IR luminosities and SFRs of galaxies at cosmological distances (e.g., Elbaz et al. 2002; Pérez-González et al. 2005; Le Floch et al. 2005). Observationally, the 12 μm luminosity is found to be a good indicator of the total IR luminosity of local galaxies (e.g., Rush et al. 1993; Elbaz et al. 2002; Takeuchi et al. 2005). The advantage of using mid-IR luminosities as indicators of the SFR is that they are not affected by the contribution from cold dust heated by old stars that may dominate the far-IR luminosities. *Spitzer* observations of nearby *normal* galaxies are now showing that there is a good correlation between the Pa α or H α luminosity (corrected for extinction) and the 24 μm luminosity of H II knots and H II regions (e.g., M51, Calzetti et al. 2005; M81, Pérez-González et al. 2006), indicating that the latter luminosity could also be a good potential SFR tracer. Calzetti et al. (2005) noted, however, that the 24 μm luminosity to SFR ratios of UV-selected starbursts and ULIRGs deviate from the average value found for the inner region of M51, suggesting that differences among different types of galaxies are likely to be present.

Figure 3 shows a comparison between the IR and the monochromatic *IRAS* 12 μm luminosities and the extinction-corrected Pa α luminosities for our sample of LIRGs. The 12 μm luminosities for close interacting systems are based on Surace et al. (2004). When they could not obtain *IRAS* fluxes for the individual components of close interacting systems, the 12 μm and IR luminosities of each component were assumed to have a ratio similar to that of their Pa α luminosities.

In addition to our sample of LIRGs, we have compiled a small comparison sample of normal galaxies with available NICMOS Pa α imaging observations (not corrected for extinction) from Böker et al. (1999). The normal galaxies were chosen so that the NICMOS Pa α observations covered the majority of the ionized hydrogen emission. If the values of the extinction inferred from H α /Pa α line ratios for a few spiral galaxies and star-forming galaxies ($A_V \sim 1$ –4 mag; see, e.g., Maoz et al. 2001; Quillen & Yukita 2001; Calzetti et al. 2005) are representative of our sample of normal galaxies, the extinction correction for the Pa α luminosity would only be up to 0.2 dex. Finally, to extend the luminosity range we have included in this comparison the four ULIRGs imaged in Pa α by Murphy et al. (2001). For the ULIRGs, the Pa α luminosities have been corrected for extinction using the A_V values these authors derived from the H α /Pa α line ratios.

There is a tight correlation between both the IR and 12 μm , and the extinction-corrected Pa α luminosities, although some of the galaxies with deviating IR luminosities (marked in the figures) seem to better follow the correlation when the 12 μm luminosity is used. For reference, in the last column of Table 6 we give the ratio between the SFRs derived from the IR luminosity and the extinction-corrected Pa α luminosity using the prescriptions of Kennicutt (1998). As can be seen from this table, for local LIRGs the SFRs derived from the number of ionizing photons are on average 0.2–0.3 dex lower than those inferred from the total IR luminosity. This behavior is consistent with the tendency for the measured IR luminosity to include some contribution from older stars (see below).

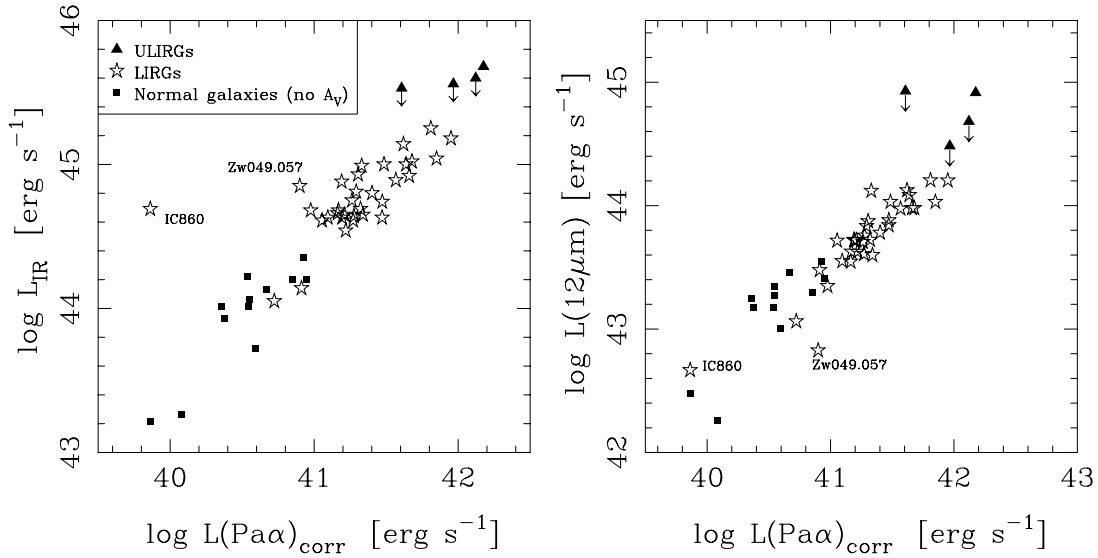


FIG. 3.—*Left*: Comparison between the IR and the extinction-corrected Pa α luminosities. For NGC 7469 we have derived the extinction-corrected Pa α luminosities of the star-forming ring from the Br γ imaging data of Genzel et al. (1995). Note that three ULIRGs of the Murphy et al. (2001) sample are not detected at 12 μ m, and thus their L_{IR} are shown as upper limits. *Right*: Comparison between the monochromatic 12 μ m and the extinction corrected Pa α luminosities. [See the electronic edition of the Journal for a color version of this figure.]

9.2. The 24 μ m Emission as a SFR Tracer for Dusty Star-forming Galaxies

We now examine in more detail the relation between mid-IR 24 μ m and Pa α luminosities. The monochromatic *IRAS* 25 μ m luminosities for our sample of LIRGs, normal galaxies, and ULIRGs have been converted to monochromatic 24 μ m luminosities using the Dale & Helou (2002) models with appropriate indices for the dust distribution (in their notation we use $\alpha = 1.5$ and $\alpha = 2$ for LIRGs and normal galaxies, respectively). In addition, we use *Spitzer* MIPS 24 μ m observations of resolved star-forming regions within the central 6 kpc region of M51 from Calzetti et al. (2005), and for M81 (entire galaxy) from Pérez-González et al. (2006). For M51, Calzetti et al. (2005) have derived the extinction corrections from H α /Pa α line ratios, and for M81 we transform the extinction-corrected (based on A_V derived from the Balmer decrement or radio) H α luminosities (see Pérez-González et al. 2006 for more details) to Pa α assuming case B recombination. The inclusion of data for resolved star-forming regions within M51 and M81 allows us to extend the range of the mid-IR–Pa α relation down 3 orders of magnitude.

As can be seen from Figure 4 (*left*), the LIRGs, ULIRGs, and normal galaxies seem to continue the relation between the extinction-corrected Pa α luminosity and the 24 μ m luminosity observed for the M51 central H II knots. We also show in this figure data for galaxies from the Universidad Complutense de Madrid sample (UCM; Pérez-González et al. 2003) and the Nearby Field Galaxy Sample (NFGS; Kewley et al. 2002) with available H α imaging, and extinction corrections derived from the Balmer decrement. These galaxies also follow the trend, but with a larger scatter, as their measurements are from H α imaging rather than Pa α . The M81 H II regions, on the other hand, follow a similar linear relation, but the relation appears to be offset with respect to that of M51, normal galaxies, and LIRGs (see discussion by Pérez-González et al. 2006). This behavior could arise from a lower UV absorption efficiency in the relatively low luminosity and lightly obscured H II regions in M81.

The best fit to the extinction-corrected Pa α versus 24 μ m luminosity relation for resolved star-forming regions of M51,

normal galaxies (with available Pa α imaging), LIRGs (excluding IC 860), and ULIRGs is

$$\log L(24 \mu\text{m}) = (-3.553 \pm 0.516) \\ + (1.148 \pm 0.013) \log L(\text{Pa}\alpha)_{\text{corr}}, \quad (1)$$

where the luminosities are in ergs s^{-1} , and the 24 μ m luminosity is computed as the monochromatic value, i.e., from νf_ν . This fit is similar to the H α versus 24 μ m relation found by Wu et al. (2005) for *Spitzer* First Look Survey star-forming galaxies. For comparison, the fit to the M51 H II regions alone gives a slightly smaller slope (1.088 ± 0.061 ; see also Calzetti et al. 2005), but within the errors of the fit including normal galaxies, LIRGs, and ULIRGs. The fit to the M81 H II regions alone provides a similar slope, essentially equal to unity (0.987 ± 0.064).

As also noted by Calzetti et al. (2005), there are variations in the mid-IR to Pa α ratios from galaxy to galaxy, clearly shown in Figure 4 (*right*). In particular, the $L(24 \mu\text{m})/L(\text{Pa}\alpha)_{\text{corr}}$ ratios of the M81 H II regions appear to follow a different trend in terms of the Pa α luminosity than the rest of galaxies and the M51 H II regions. [Pérez-González et al. 2006 attribute the large scatter of $L(24 \mu\text{m})/L(\text{Pa}\alpha)_{\text{corr}}$ in M81 to uncertain extinction corrections]. The variation of the $L(24 \mu\text{m})/L(\text{Pa}\alpha)_{\text{corr}}$ ratio with the Pa α luminosity (i.e., SFR) between the M51 H II knots and our LIRGs and ULIRGs is similar to the $L(24 \mu\text{m})/\text{SFR}$ ratios found by Calzetti et al. (2005). In fact, the gap between the M51 H II knots and the LIRGs/ULIRGs seen in our figure is occupied by their UV-selected sample of starbursts, and the UCM and NFGS galaxies. We note, however, that we find a more pronounced variation of the $L(24 \mu\text{m})/L(\text{Pa}\alpha)_{\text{corr}}$ ratio because we use the Pa α luminosity as a proxy for the SFR for LIRGs, whereas they use the IR luminosity (see previous section, and Table 6).

9.2.1. Deeply Embedded Sources

The deviation from strict proportionality in the $L(24 \mu\text{m})$ versus $L(\text{Pa}\alpha)_{\text{corr}}$ relation in dusty systems probably results from the effects of extinction. LIRGs and ULIRGs are known to contain highly obscured regions, usually associated with the nuclei

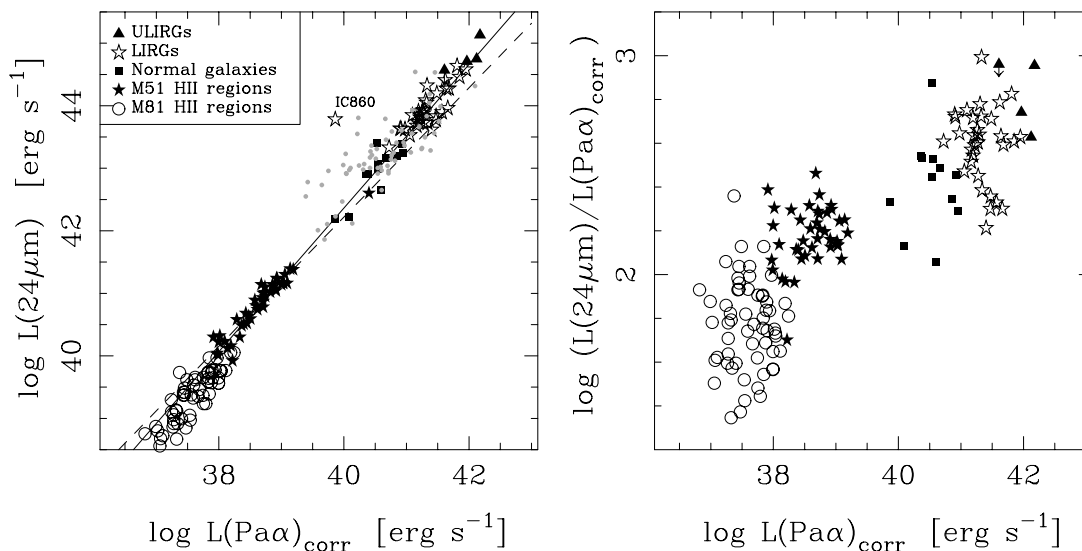


FIG. 4.—*Left*: Monochromatic $24\ \mu\text{m}$ luminosities vs. extinction-corrected $\text{Pa}\alpha$ luminosities for our sample of LIRGs, as well as normal galaxies and ULIRGs (those shown in Fig. 3). We also show data for individual star-forming regions within two nearby galaxies with *Spitzer* MIPS $24\ \mu\text{m}$ observations. For M51 the Calzetti et al. (2005) $\text{Pa}\alpha$ observations cover the central 6 kpc of the galaxy. For M81 (see Pérez-González et al. 2006) the $\text{H}\alpha$ observations include the entire galaxy, and have been converted to $\text{Pa}\alpha$ luminosities assuming case B recombination. The solid line is the derived fit to the M51 knots, normal galaxies, LIRGs (excluding IC 860), and ULIRGs (see text). For comparison, the dashed line shows the fit to the M51 H II knots given in Calzetti et al. (2005). Note how star-forming galaxies from the UCM and NFGS surveys (gray dots; not included in the fit) also follow the trend. *Right*: Ratio of the $24\ \mu\text{m}$ to extinction-corrected $\text{Pa}\alpha$ luminosities vs. the extinction-corrected $\text{Pa}\alpha$ luminosity. We only show galaxies with $\text{Pa}\alpha$ imaging data, that is, the UCM and NFGS galaxies are excluded. Symbols are as in left panel. [See the electronic edition of the Journal for a color version of this figure.]

of the galaxies, that are optically thick in the optical, and even in the near- and mid-IR (e.g., Genzel et al. 1995, 1998; Alonso-Herrero et al. 2000; Doyon et al. 1994; Kotilainen et al. 1996; Zhou et al. 1993). There is also indirect evidence based on the observed ratios of mid-IR fine-structure emission lines that many of the youngest stars in massive starbursts may still be embedded in ultracompact high-density H II regions (Rigby & Rieke 2004) and thus may be hidden from us by large amounts of extinction.

The departures from a constant $L(24\ \mu\text{m})/L(\text{Pa}\alpha)_{\text{corr}}$ ratio may be linked to differences in the physical conditions in regions experiencing intense star formation. In particular, the average extinction for the H II regions in M81 is $A_V \sim 0.8$ mag (Pérez-González et al. 2006), whereas for the H II knots of M51 it is $A_V \sim 3.5$ mag (Calzetti et al. 2005), and for our sample of LIRGs the average extinctions over the $\text{Pa}\alpha$ -emitting regions are $A_V \sim 2\text{--}6$ mag.

Since the estimated extinctions for the M51 H II regions and LIRGs are not too different, it is possible that we are underestimating the extinction in our sample of LIRGs. As shown for Arp 299 by Alonso-Herrero et al. (2000) and for NGC 7469 by Genzel et al. (1995), the $J - H$ continuum colors tend to underestimate the extinction in very dusty systems. Thus, it is possible that the photometric extinctions derived for some of the galaxies in our sample are only lower limits to the true extinction (e.g., compare the photometric and spectroscopic extinctions to the central regions of IRAS 17138–1017 and NGC 2388). In particular this may be the case for the $\text{Pa}\alpha$ emission in highly inclined dusty galaxies (those described in § 5.5). We note also that not all of the most luminous IR systems in our sample are dominated by such extinguished sources; for instance, the star formation properties of the merger NGC 1614 can be explained with $A_K \simeq 0.5$ mag (see Alonso-Herrero et al. 2001). Fortunately, the relative insensitivity of $\text{Pa}\alpha$ to extinction makes these differences relatively unimportant in estimating the SFR, or the scatter in Figure 4 would be much larger than it is.

The high extinction indicated for the LIRGs, the possibility that the extinction is actually higher than our estimates, and the likelihood that some of the youngest stars are still embedded in ultracompact H II regions are all consistent with our finding of a slope of the $L(24\ \mu\text{m})$ versus $L(\text{Pa}\alpha)_{\text{corr}}$ relation significantly larger than unity. We believe that the physical explanation for this behavior is that the dust competes increasingly effectively for ionizing photons and ultraviolet continuum photons in very heavily obscured systems, so that there is a trend for an increasing fraction of the luminosity to emerge in the IR. A surprising result, however, is that this trend is so similar from galaxy to galaxy. For reasonably dust embedded galaxies and H II regions, there is a linear empirical relationship between IR and hydrogen recombination luminosity with very small scatter that holds over more than 4 decades in luminosity.

9.2.2. Presence of AGN Emission

The presence of a bright AGN could make a significant contribution to the mid-IR luminosity of a system. Approximately 25% of the galaxies are classified as AGN (Seyfert or LINER) on the basis of optical line ratios (see Table 1). Three additional LIRGs (ESO 320-G030, IC 860, and Zw 049.057) present megamaser emission (Norris et al. 1986; Baan et al. 1993). In extragalactic sources, megamaser emission is generally associated with a strong compact radio continuum source, and about 70% of megamaser sources are classified as AGN or composite sources from optical spectroscopy (Baan et al. 1998), or tend to appear in galaxies with warmer *IRAS* colors (Baan et al. 1993). Including the galaxies with megamaser emission the fraction of AGNs in our sample is consistent with that derived by other works (e.g., Veilleux et al. 1995; Tran et al. 2001) for the same IR luminosity range.

For NGC 7469, Genzel et al. (1995) estimated that the nucleus contributes up to 40% of *IRAS* IR luminosity (see also Soifer et al. 2003). For the B1 nucleus (classified as a Seyfert) of NGC 3690, Keto et al. (1997) estimated a contribution of 20%–30% in the mid-IR. For the rest of the galaxies in our sample containing

an AGN, only in the case of IC 4518W do we find that the Seyfert nucleus dominates the observed mid-IR emission (see A. Alonso-Herrero et al. 2006, in preparation).

Kewley et al. (2000) have argued, based on the radio properties of a sample of warm IR galaxies with IR luminosities similar to our sample, that in the cases where an AGN is detected spectroscopically, it is rarely the dominant power source for the IR luminosity. In most cases, in the galaxies in our sample containing an AGN there is extended H II emission over large scales (e.g., NGC 7130, NGC 3690), so it is likely that the AGN contribution to the total IR luminosity of the system is significantly smaller than in the case of NGC 7469 and IC 4518W.

9.2.3. Empirical Calibration

We can use the relation in equation (1) for empirical estimates of the SFR in dusty environments. The most direct application is to calculate the intrinsic extinction-corrected Pa α luminosity from the monochromatic luminosity at 24 μ m. Inverting equation (1), we find

$$L(\text{Pa}\alpha)_{\text{corr}} = 1244 L(24 \mu\text{m})^{0.871}. \quad (2)$$

Kennicutt (1998) derived a relationship between H α luminosity and the SFR. He also converted this expression to one between total IR luminosity and SFR in dusty galaxies, and this latter expression has been widely used to interpret IR observations. We now update the expression based on the results reported in this paper. First, we use monochromatic 24 μ m luminosities in place of total IR luminosities. Kennicutt (1998) assumed in deriving his relationship that the great majority of the luminosity from young stars would be absorbed by dust and reradiated in the far-IR. Although this assumption is likely to be correct, observationally there may be other contributions to the total IR luminosity from older populations of stars or other luminosity sources (e.g., review by Tuffs & Popescu 2005). Therefore, a true total IR luminosity measurement may overestimate the recent star formation in a galaxy, although estimates based on *IRAS* measurements alone are less subject to these considerations, because they only poorly sample the output of the cold dust (because the longest band is at 100 μ m). Second, Kennicutt assumed a direct proportionality between the H α luminosity and the total IR. We find empirically that the increasing absorption efficiency in increasingly luminous and obscured galaxies leads to a deviation from strict proportionality toward increasing IR output with increasing star-forming luminosity.

We begin by calibrating the mid-IR/Pa α relation using the H II regions in M51. The extinction to these regions is roughly 2 mag at H α . Since the morphologies are similar between H α and Pa α (Quillen & Yukita 2001), a straightforward extinction correction is appropriate (e.g., there are minimal issues with very heavily obscured regions that contribute no H α). Assuming case B recombination, the relation between SFR and H α quoted by Kennicutt (1998) can be converted to $\text{SFR}(M_{\odot} \text{ yr}^{-1}) = 6.79 \times 10^{-41} L(\text{Pa}\alpha)$ (ergs s $^{-1}$). From these considerations, we derive the following relation between the SFR rate and mid-IR luminosity for luminous, dusty galaxies:

$$\text{SFR}(M_{\odot} \text{ yr}^{-1}) = 8.45 \times 10^{-38} \left[\frac{L(24 \mu\text{m})}{\text{ergs s}^{-1}} \right]^{0.871}. \quad (3)$$

This relation is analogous to the widely used relation between SFR and IR luminosity (Kennicutt 1998), but it is not affected by the uncertain contribution to the total IR luminosity of a galaxy of dust heating from old stars.

10. SUMMARY

We have analyzed *HST* NICMOS 1.1–1.89 μ m continuum and Pa α emission line observations of a volume-limited sample of 30 local universe LIRGs ($\log L_{\text{IR}} = 11\text{--}11.9 [L_{\odot}]$). The galaxies have been selected so that the Pa α emission line could be observed with the NICMOS F190N narrowband filter ($2800 < v < 5200 \text{ km s}^{-1}$). The sample comprises approximately 80% of all the LIRGs in the RBGS in the above velocity interval, and is representative of local LIRGs in general. The NICMOS observations cover the central $\simeq 3.3\text{--}7.2 \text{ kpc}$ of the galaxies. We find the following:

1. The most common morphological continuum features in the central regions are bright star clusters and large-scale spiral arms, sometimes extending down to the inner kpc (minispirals). In highly inclined systems, there are dust lanes crossing the disks of the galaxies and in some cases even hiding the nucleus of the galaxy. The “extreme” (perturbed) morphologies commonly seen in ULIRGs are only observed in some of the most IR-luminous examples in our sample.

2. Approximately half of the LIRGs show compact ($\sim 1\text{--}2 \text{ kpc}$) Pa α morphologies in the form of nuclear star formation rings, minispiral structure, and emission associated with the nucleus of the galaxy. The typical observed (not corrected for extinction) H α surface brightnesses are in the range $2\text{--}10 \times 10^{41} \text{ ergs s}^{-1} \text{ kpc}^{-2}$, although the most extreme cases, for instance the ring of star formation of NGC 1614, can reach $\simeq 60 \times 10^{41} \text{ ergs s}^{-1} \text{ kpc}^{-2}$.

3. The remaining half of the galaxies show Pa α emission extending over scales of $\simeq 3.3\text{--}7.2 \text{ kpc}$ and larger, with bright H II regions in the spiral arms (face-on systems) or along the disks of the galaxies (edge-on systems), with or without bright nuclear emission. The H α surface brightnesses are about 1 order of magnitude fainter than in galaxies with compact Pa α emission.

4. Most of the LIRGs show a population of numerous bright H II regions, and in about half of them the typical H II region (the median H α luminosity) is as bright as or brighter than the giant H II region 30 Dor. The most IR (as well as in H α) luminous galaxies tend to host the brightest median and first-ranked H II regions.

5. The extinctions to the gas (derived from the H α /Pa α and Pa α /Br γ line ratios) and to the stars (derived from the $m_{\text{F110W}} - m_{\text{F160W}}$ colors) are on average $A_V \sim 2\text{--}6 \text{ mag}$ over the Pa α -emitting regions covered by the *HST* NICMOS images.

6. There exists a good correlation between the mid-IR 24 μ m and the extinction-corrected Pa α luminosities of LIRGs, ULIRGs, normal galaxies, and H II regions of M51, covering nearly 5 decades in luminosity. This suggests that the mid-IR luminosity of galaxies undergoing dusty, intense star formation is a good indicator of the SFR. The increasing $L(24 \mu\text{m})/L(\text{Pa}\alpha)_{\text{corr}}$ ratio for more luminous Pa α emitters (that is, galaxies with higher SFRs) may be due to the presence of deeply embedded sources in the youngest star-forming regions, for which we have underestimated the extinction, even at near-IR wavelengths.

7. Analogous to the widely used relation between SFR and total IR luminosity (Kennicutt 1998), we show that SFRs can be determined accurately in luminous, dusty galaxies as $\text{SFR}(M_{\odot} \text{ yr}^{-1}) = 8.45 \times 10^{-38} [L(24 \mu\text{m})/(\text{ergs s}^{-1})]^{0.871}$.

Based on observations with the NASA/ESA *Hubble Space Telescope* at the Space Telescope Science Institute, which is operated by the Association of Universities for Research in Astronomy, Inc., under NASA contract NAS 5-26555. This research has made use of the NASA/IPAC Extragalactic Database (NED),

which is operated by the Jet Propulsion Laboratory, California Institute of Technology, under contract with the National Aeronautics and Space Administration (NASA).

We thank an anonymous referee for a careful reading of the manuscript and useful suggestions. We would like to thank D. Calzetti and R. Kennicutt for enlightening discussions. We are grateful to T. Hattori for providing us with $H\alpha$ images of the galaxies. We thank T. Díaz-Santos for helping us with the *Spitzer*

MIPS images of the sample of LIRGs. A. A. H. and L. C. acknowledge support from the Spanish Programa Nacional de Astronomía y Astrofísica under grant AYA2002-01055 and Plan Nacional del Espacio ESP2005-01480, and PGP from the Spanish Programa Nacional de Astronomía y Astrofísica under grant AYA 2004-01676. This work has been funded by NASA grant HST-GO-10169 and by NASA through contract 1255094 issued by JPL/Caltech.

REFERENCES

- Alonso-Herrero, A., Engelbracht, C. W., Rieke, M. J., Rieke, G. H., & Quillen, A. C. 2001, *ApJ*, 546, 952
- Alonso-Herrero, A., & Knapen, J. H. 2001, *AJ*, 122, 1350
- Alonso-Herrero, A., Rieke, G. H., Rieke, M. J., & Scoville, N. Z. 2000, *ApJ*, 532, 845
- . 2002, *AJ*, 124, 166
- Arribas, S., Bushouse, H., Lucas, R. A., Colina, L., & Borne, K. D., et al. 2004, *AJ*, 127, 2522
- Baan, W. A., Haschick, A. D., & Uglesich, R. 1993, *ApJ*, 415, 140
- Baan, W. A., Salzer, J. J., & LeWinter, R. D. 1998, *ApJ*, 509, 633
- Beckman, J. E., Rozas, M., Zurita, A., Watson, R. A., & Knapen, J. H. 2000, *AJ*, 119, 2728
- Bell, E. F., et al. 2005, *ApJ*, 625, 23
- Bertin, E., & Arnouts, S. 1996, *A&AS*, 117, 393
- Bland-Hawthorn, J., & Maloney, P. R. 1999, *ApJ*, 510, L33
- Böker, T., Sarzi, M., McLaughlin, D. E., van der Marel, R., Rix, H.-W., Ho, L. C., & Shields, J. C. 2004, *AJ*, 127, 105
- Böker, T., et al. 1999, *ApJS*, 124, 95
- Bushouse, H. A., Borne, K. D., Colina, L., Lucas, R. A., Rowan-Robinson, M., Baker, A. C., Clements, D. L., Lawrence, A., & Oliver, S. 2002, *ApJS*, 138, 1
- Calzetti, D., Kinney, A. L., & Storchi-Bergmann, T. 1994, *ApJ*, 429, 582
- Calzetti, D., et al. 2005, *ApJ*, 633, 871
- Clements, D. L., Sutherland, W. J., McMahon, R. G., & Saunders, W. 1996, *MNRAS*, 279, 477
- Colina, L., Arribas, S., & Clements, D. 2004, *ApJ*, 602, 181
- Colina, L., Borne, K., Bushouse, H., Lucas, R. A., Rowan-Robinson, M., Lawrence, A., Clements, D., Baker, A., & Oliver, S. 2001, *ApJ*, 563, 546
- Corbett, E. A., Kewley, L., Appleton, P. N., Charmandaris, V., Dopita, M. A., Heisler, C. A., Norris, R. P., Zezas, A., & Marston, A. 2003, *ApJ*, 583, 670
- Dale, D. A., & Helou, G. 2002, *ApJ*, 576, 159
- Dopita, M. A., Pereira, M., Kewley, L. J., & Capaccioli, M. 2002, *ApJS*, 143, 47
- Doyon, R., Joseph, R. D., & Wright, G. S. 1994, *ApJ*, 421, 101
- Elbaz, D., Cesarsky, C. J., Chantal, P., Aussel, H., Franceschini, A., Fadda, D., & Chary, R. R. 2002, *A&A*, 384, 848
- García-Marín, M., Colina, L., Arribas, S., Alonso-Herrero, A., & Mediavilla, E. 2006, *ApJ*, submitted
- Gehrz, R. D., Sramek, R. A., & Weedman, D. W. 1983, *ApJ*, 267, 551
- Genzel, R., Weitzel, L., Tacconi-Garman, L. E., Blietz, M., Cameron, M., Krabbe, A., Lutz, D., & Sternberg, A. 1995, *ApJ*, 444, 129
- Genzel, R., et al. 1998, *ApJ*, 498, 579
- . 2001, *ApJ*, 563, 527
- Goldader, J. D., Joseph, R. D., Doyon, R., & Sanders, D. B. 1997a, *ApJS*, 108, 449
- . 1997b, *ApJ*, 474, 104
- Hattori, T., Yoshida, M., Ohtani, H., Sugai, H., Ishigaki, T., Sasaki, M., Hayashi, T., Ozaki, S., Ishii, M., & Kawai, A. 2004, *AJ*, 127, 736
- Hummer, D. G., & Storey, P. J. 1987, *MNRAS*, 224, 801
- Kennicutt, R. C., Jr. 1998, *ARA&A*, 36, 189
- Kennicutt, R. C., Jr., Edgar, B. K., & Hodge, P. W. 1989, *ApJ*, 337, 761
- Keto, E., et al. 1997, *ApJ*, 485, 598
- Kewley, L. J., Geller, M. J., Jansen, R. A., & Dopita, M. A. 2002, *AJ*, 124, 3135
- Kewley, L. J., Heisler, C. A., Dopita, M. A., & Lumsden, S. 2001, *ApJS*, 132, 37
- Kewley, L. J., Heisler, C. A., Dopita, M. A., Sutherland, R., Norris, R. P., Reynolds, J., & Lumsden, S. 2000, *ApJ*, 530, 704
- Kim, D.-C., Sanders, D. B., Veilleux, S., Mazzarella, J. M., & Soifer, B. T. 1995, *ApJS*, 98, 129
- Kotilainen, J. K., Moorwood, A. F. M., Ward, M. J., & Forbes, D. A. 1996, *A&A*, 305, 107
- Lagache, G., Puget, J.-L., & Dole, H. 2005, *ARA&A*, 43, 727
- Le Floc'h, E., et al. 2005, *ApJ*, 632, 169
- Lehnert, M. D., & Heckman, T. M. 1995, *ApJS*, 97, 89
- Lípári, S., Díaz, R. J., Forte, J. C., Terlevich, R., Taniguchi, Y., Aguero, M. P., Alonso-Herrero, A., Mediavilla, E., & Zepf, S. 2004, *MNRAS*, 354, L1
- Lípári, S., Díaz, R., Taniguchi, Y., Terlevich, R., Dottori, H., & Carranza, G. 2000, *AJ*, 120, 645
- Maoz, D., Barth, A. J., Ho, L. C., Sternberg, A., & Filippenko, A. V. 2001, *AJ*, 121, 3048
- Márquez, I., Moles, M., & Masegosa, J. 1996, *A&A*, 310, 401
- Martini, P., Regan, M. W., Mulchaey, J. S., & Pogge, B. W. 2003, *ApJ*, 589, 774
- McLeod, K. K., Rieke, G. H., Rieke, M. J., & Kelly, D. M. 1993, *ApJ*, 412, 111
- Melbourne, J., Koo, D. C., & Le Floc'h, E. 2005, *ApJ*, 632, L65
- Melbourne, J., & Salzer, J. J. 2002, *AJ*, 123, 2302
- Miles, J. W., Houck, J. R., Hayward, T. L., & Ashby, M. L. N. 1996, *ApJ*, 465, 191
- Murphy, T. W., Soifer, B. T., Matthews, K., & Armus, L. 2001, *ApJ*, 559, 201
- Murphy, T. W., Jr., Armus, L., Matthews, K., Soifer, B. T., Mazzarella, J. M., Shupe, D. L., Strauss, M. A., & Neugebauer, G. 1996, *AJ*, 111, 1025
- Norris, R. P., Whiteoak, J. B., Gardner, F. F., Allen, D. A., & Roche, P. F. 1986, *MNRAS*, 221, 51P
- Papovich, C., Egami, E., Le Floc'h, E., Pérez-González, P., Rieke, G., Rigby, J., Dole, H., & Rieke, M. 2005, in *Planets to Cosmology: Essential Science in Hubble's Final Years*, in press (astro-ph/0408454)
- Pérez-González, P. G., Zamorano, J., Gallego, J., Aragón-Salamanca, A., & Gil de Paz, A. 2003, *ApJ*, 591, 827
- Pérez-González, P. G., et al. 2005, *ApJ*, 630, 82
- . 2006, *ApJ*, in press
- Quillen, A. C., McDonald, C., Alonso-Herrero, A., Lee, A., Shaked, S., Rieke, M. J., & Rieke, G. H. 2001, *ApJ*, 547, 129
- Quillen, A. C., & Yukita, M. 2001, *AJ*, 121, 2095
- Rieke, G. H., & Lebofsky, M. J. 1985, *ApJ*, 288, 618
- Rieke, G. H., Loken, K., Rieke, M. J., & Tamblyn, P. 1993, *ApJ*, 412, 99
- Rieke, G. H., & Low, F. J. 1972, *ApJ*, 176, L95
- Rigby, J. R., & Rieke, G. H. 2004, *ApJ*, 606, 237
- Roy, A. L., Goss, W. M., Mohan, N. R., & Anantharamaiah, K. R. 2005, *A&A*, 435, 831
- Rush, B., Malkan, M. A., & Spinoglio, L. 1993, *ApJS*, 89, 1
- Sanders, D. B., Egami, E., Lípári, S., Mirabel, I. F., & Soifer, B. T. 1995, *AJ*, 110, 1993
- Sanders, D. B., Mazzarella, J. M., Kim, D.-C., Surace, J. A., & Soifer, B. T. 2003, *AJ*, 126, 1607
- Sanders, D. B., & Mirabel, I. F. 1996, *ARA&A*, 34, 749
- Sanders, D. B., Soifer, B. T., Elias, J. H., Neugebauer, B., & Matthews, K. 1988, *ApJ*, 328, L35
- Satyapal, S., Watson, D. M., Pipher, J. L., Forrest, W. J., Fischer, J., Greenhouse, M. A., Smith, H. A., & Woodward, C. E. 1999, *ApJ*, 516, 704
- Scoville, N. Z., Poletta, M., Ewald, S., Stolovy, S. R., Thompson, R., & Rieke, M. J. 2001, *AJ*, 122, 3017
- Scoville, N. Z., et al. 2000, *AJ*, 119, 991
- Sekiguchi, K., & Wolstencroft, R. D. 1992, *MNRAS*, 255, 581
- Shi, Y., Rieke, G. H., Papovich, C., Pérez-González, P. G., & Le Floc'h, E. 2006, *ApJ*, 645, 199
- Soifer, B. T., Bock, J. J., Marsh, K., Neugebauer, G., Matthews, K., Egami, E., & Armus, L. 2003, *AJ*, 126, 143
- Soifer, B. T., Neugebauer, G., Matthews, K., Egami, E., Weinberger, A. J., Ressler, M., Scoville, N. Z., Stolovy, S. R., Condon, J. J., & Becklin, E. E. 2001, *AJ*, 122, 1213
- Soifer, B. T., Sanders, D. B., Madore, B. F., Neugebauer, G., Danielson, G. E., Elias, J. H., Lonsdale, C. J., & Rice, W. L. S. 1987, *ApJ*, 320, 238
- Sugai, H., Davies, R. I., Malkan, M. A., McLean, I. S., Usuda, T., & Ward, M. J. 1999, *ApJ*, 527, 778
- Surace, J. A., Sanders, D. B., & Evans, A. S. 2000, *ApJ*, 529, 170
- Surace, J. A., Sanders, D. B., & Mazzarella, J. M. 2004, *AJ*, 127, 3235
- Takeuchi, T. T., Buat, V., Iglesias-Páramo, J., Boselli, A., & Burgarella, D. 2005, *A&A*, 432, 423
- Tran, Q. D., et al. 2001, *ApJ*, 552, 527

- Tuffs, R. J., & Popescu, C. C. 2005, AIP Conf. Ser. 761, The Spectral Energy Distributions of Gas-rich Galaxies: Confronting Models with Data, ed. C. C. Popescu & R. J. Tuffs (Berlin: Springer), 344
- van den Broek, A. C., et al. 1991, A&AS, 91, 61
- Veilleux, S., Kim, D.-C., Sanders, D. B., Mazzarella, J. M., & Soifer, B. T. 1995, ApJS, 98, 171
- Véron-Cetty, M.-P., & Véron, P. 2001, A&A, 374, 92
- Witt, A. N., & Gordon, K. D. 2000, ApJ, 528, 799
- Wu, H., Zou, Z. L., Xia, X. Y., & Deng, Z. G. 1998, A&AS, 132, 181
- Wu, H., et al. 2005, ApJ, 632, L79
- Wynn-Williams, C. G., & Becklin, E. E. 1993, ApJ, 412, 535
- Zhao, J.-H., Anantharamaiah, K. R., Goss, W. M., & Viallefond, F. 1997, ApJ, 482, 186
- Zheng, X. Z., Hammer, F., Flores, H., Assémat, F., & Pelat, D. 2004, A&A, 421, 847
- Zhou, S., Wynn-Williams, C. G., & Sanders, D. B. 1993, ApJ, 409, 149